

Supplement A. Sensitivity of cone heating model to variation in cone properties at 345.32 and 1221.27 degree days.

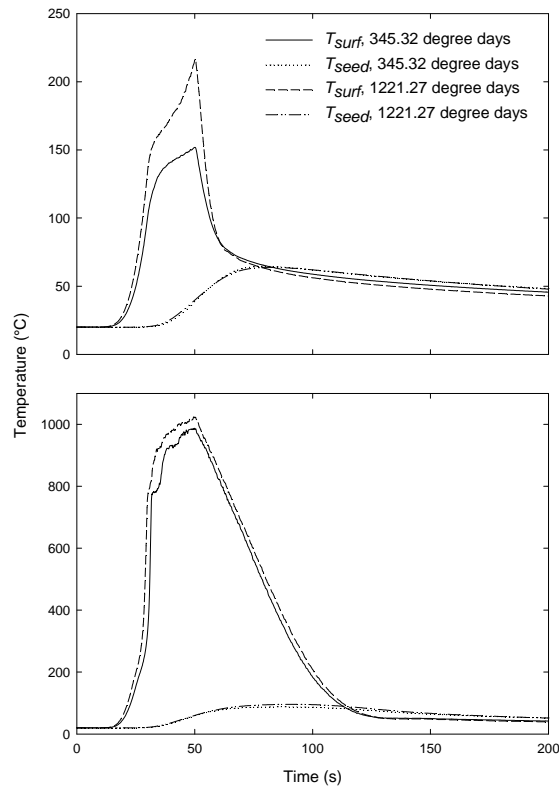


Figure A1: Sensitivity of cone heating model to variation in cone properties at 345.32 and 1221.27 degree days. Cones were heated in two plumes that produced time series of surface temperatures similar to those observed in simulated forest fires (Fig. 4). Maximum seed temperatures for cone properties at 345.32 and 1221.27 degree days varied by 1.2 % (top) and 9.37 % (bottom), so mean cone properties calculated over the entire sampling period were used for subsequent simulations.

Supplement B. Mean (\pm SEM) physical properties of cones as a function of accumulated degree days from ordinal day 1.

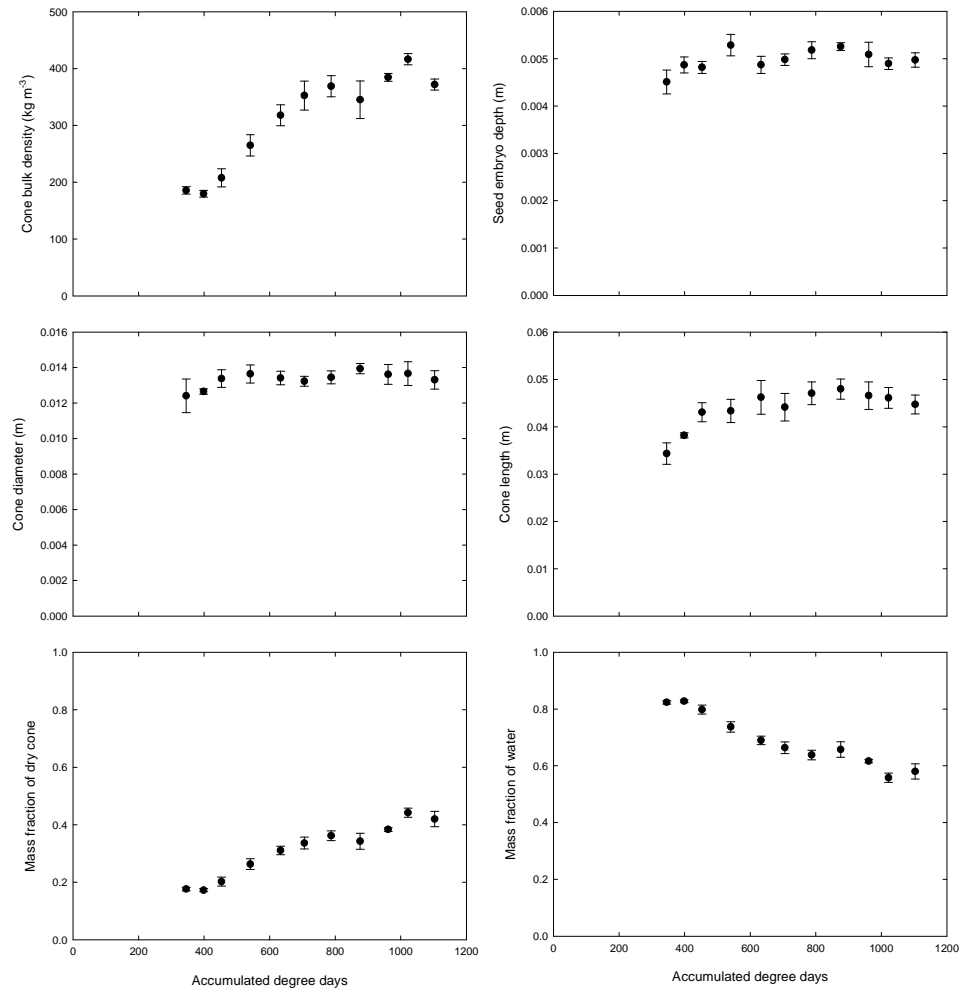


Figure B1: Mean (\pm SEM) physical properties of cones as a function of accumulated degree days from ordinal day 1. Data are consistent with those reported for white spruce at Chalk River, Ontario (Winston and Haddon, 1981).

Supplement C. Insensitivity of simulated seed temperatures to changes in computational grid resolution.

The highest frequency heat flux oscillation that can be resolved in a WFDS simulation, f , is given by

$$f = \frac{1}{2\Delta t} \quad (\text{C0})$$

Since the timestep Δt varies with grid cell size according to the Courant-Friedrichs-Lewy (CFL) stability criterion (McGrattan et al., 2010), the highest frequency heat flux oscillation is ultimately determined by the size of the computational grid cells.

Cone heating is driven by the net heat flux incident on the cone's surface. White spruce cones are thermally thick, so seed temperature will only respond to changes in surface flux below a certain frequency; for changes in surface flux above this frequency, seed temperature will not respond.

To show that an increase in computational grid resolution would not change the results of our cone heating simulations (i.e., Figs. 4-5), we conducted test simulations of cone heating in response to prescribed sinusoidal heat fluxes characterized by frequencies above and below the highest resolved frequency in our WFDS crown fire simulations. Power spectra of surface flux time histories did not reveal a dominant frequency, so Eq. (C0) was used to calculate the highest potential frequency resolved in the simulations (141.24 Hz); for this calculation, Δt taken as the smallest value observed in the simulations (0.00354 s). Next, we considered cone heating in response to prescribed sinusoidal heat fluxes of four frequencies: 0.05 Hz, 70.62 Hz (half of the highest potential frequency in the simulated crown fires), 141.24 Hz (the highest potential frequency in the simulated crown fires), and 282.49 Hz (twice the highest potential frequency in

the simulated crown fires). Although these four frequencies correspond to different grid cell sizes according to Eq. (C0) and the CFL criterion, here the calculation required only the sinusoidal surface flux history and not the gas phase calculations that would produce them. Each simulation was run for 60 s, which is equal to 3 times the period of the lowest frequency sine wave (0.05 Hz). Simulations shared a common time step of 0.000354 s, which is equal to 1/10 of the period of the highest frequency wave (282.49 Hz). Oscillations in prescribed heat flux had a mean value of zero, so seed temperatures would only change for lower frequency oscillations to which cone heating could respond, and would not change for higher frequency oscillations to which cone heating could not respond. Temperatures at the cone surface and seed locations were expressed as the normalized temperature θ

$$\theta = \frac{T_t}{T_0} - 1 \quad (\text{C0})$$

where T_t is the temperature at time t and T_0 is the temperature at time $t = 0$, which is the same for all cases. If seed temperature can respond to the prescribed sinusoidal heat flux, this normalized temperature will vary; if not, it will remain at a constant value of 0.

Prescribed surface heat flux histories and resultant surface and seed temperature histories are shown in Figure C1. The seed temperature did not respond to sinusoidal variation in surface heat flux with a frequency equal to the highest potential frequency resolved in our crown fire simulations (141.24 Hz; Figs. C1e - C1f). Likewise, seed temperature did not respond to heat flux oscillations with a frequency of twice the maximum value resolved in the crown fire simulations (141.24 Hz; Figs. C1g - C1h), so that (all else being equal) seed temperatures would not respond to an increase in computational grid resolution. Seed temperature also did not respond to flux oscillations with a frequency of one-half the maximum value resolved in the simulations (70.62 Hz; Figs. C1c - C1d), meaning that the grid resolution of our crown fire

simulations is much higher than is necessary for the cone heating model response. Indeed, it was only for the extremely low frequency heat flux considered here (0.005 Hz) that the seed temperature responded (Figs. C1a - C1b), and heat flux oscillations with these frequencies were resolved in the simulations.

In summary, these test simulations demonstrate that seed temperatures were insensitive to oscillations of the net incident heat flux with frequencies that could potentially occur in a higher resolution grid. Thus, if the simulations were rerun with a finer grid, resulting in heat flux time histories with higher frequency components, the thermal response of the cone would be unchanged.

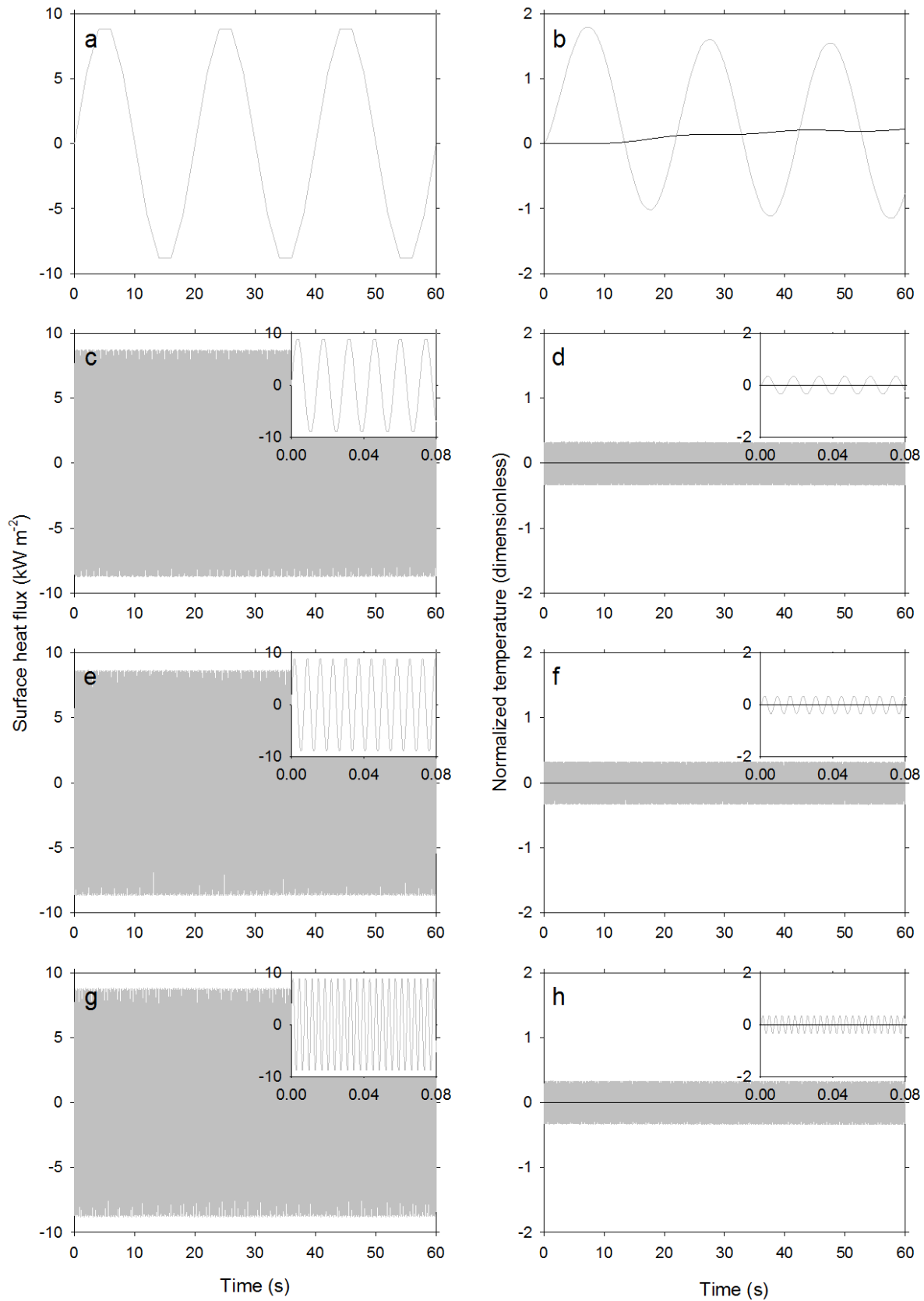


Figure C1: Sensitivity of simulated seed temperature in response to changes in frequency of cone surface heat flux oscillations. Time series of heat flux (a,c,e,g) and temperature (b,d,f,h) for cone surfaces (grey lines) and seeds (black line) across 60 s (main panel) and 0.08 s (insets) time intervals. Frequencies of cone surface heat flux oscillations were taken as 0.05 Hz (a,b), 70.62 Hz (half of the highest frequency resolved in our crown fire simulations; c,d), 141.24 Hz (the highest frequency resolved in our crown fire simulations; e,f), and 282.49 (twice the highest frequency resolved in our crown fire simulations; g,h). Grey areas result from compressed line plots for high frequencies when the time interval is large.

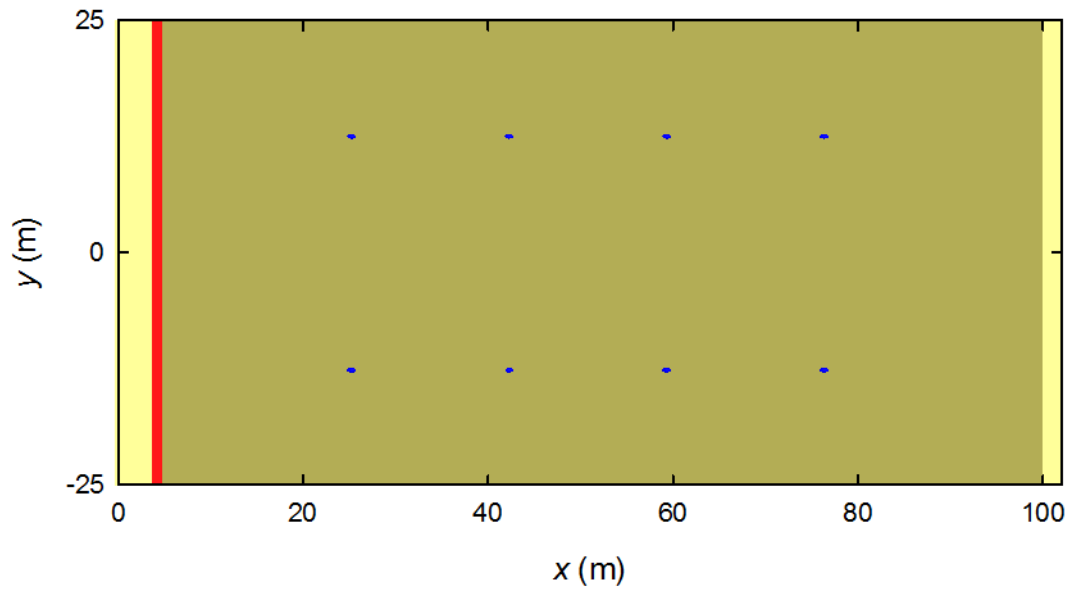
Supplement D. Plan view of computational domain.

Figure D1: Plan view of computational domain showing locations of ignition source (red), surface fuelbed (brown), and vertical cone arrays (blue ellipsoids; not to scale).

Supplement E. Vertical wind profile prescribed at $x = 0$.

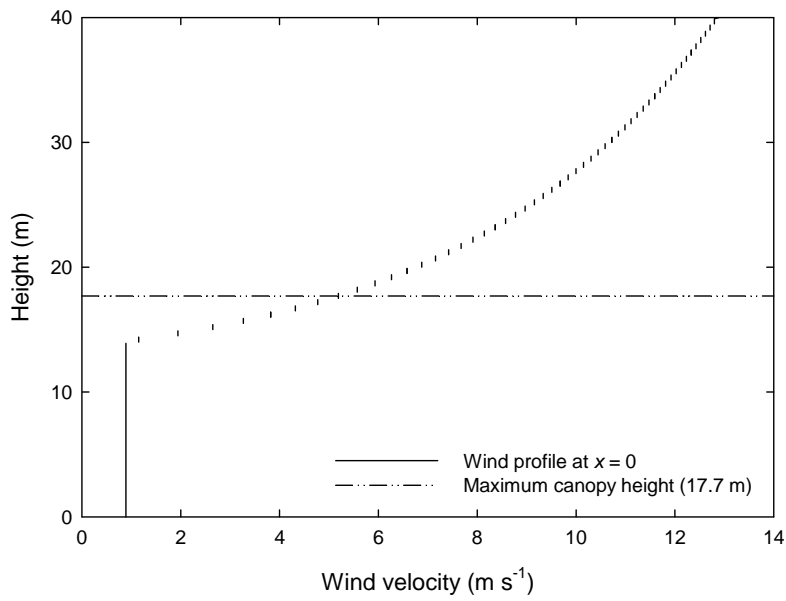


Figure E1: Vertical wind profile prescribed at $x = 0$ (Albini and Baughman, 1979). Discontinuities reflect averaging of wind velocity over discrete 0.5 m height increments.

Supplement F. Typical u -velocities at the $y = 0$ plane in the absence of fire.

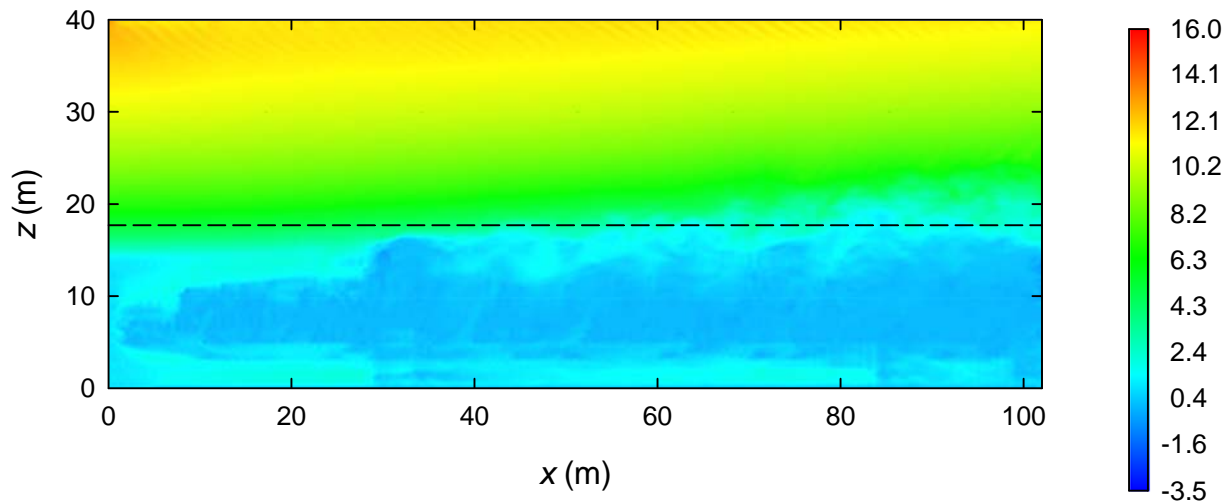


Figure F1: Typical u -velocities (m/s) at the $y = 0$ plane in the absence of fire. A time-averaged wind profile is prescribed at $x = 0$ (see Eqn. 8 and Figure E1; Albini and Baughman, 1979)).

Dashed line indicates the maximum canopy height of $z = 17.7$ m.

Supplement G. Maximum seed temperature for cones in five simulated forest fires.

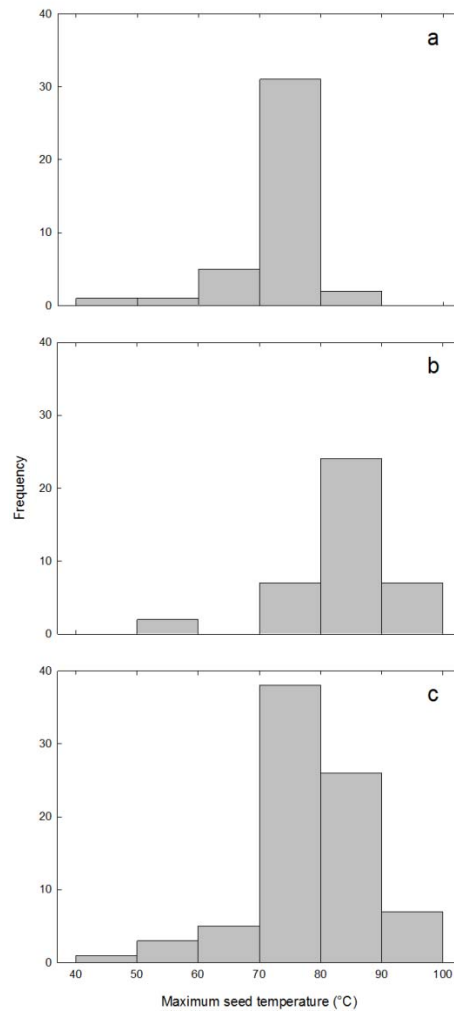


Figure G1: Maximum seed temperature for cones in five simulated forest fires at heights $z = 17.7$ m (a), $z = 8.7$ m (b), and $z = 17.7$ and 8.7 m combined (c).

Supplement H. Maximum seed temperature in cones plotted against time-integrated total heat flux.

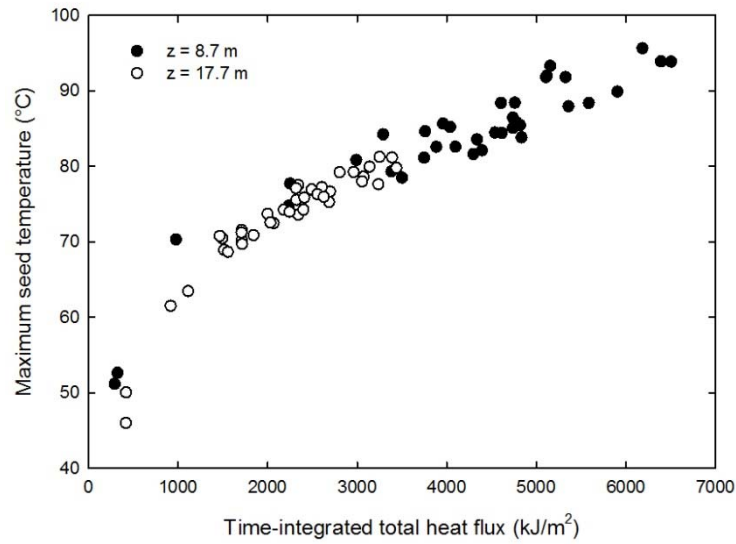


Figure H1: Maximum seed temperature in cones plotted against time-integrated total heat flux.

Each point is an individual cone.

Supplement I. Timing of fire occurrence and seed development.

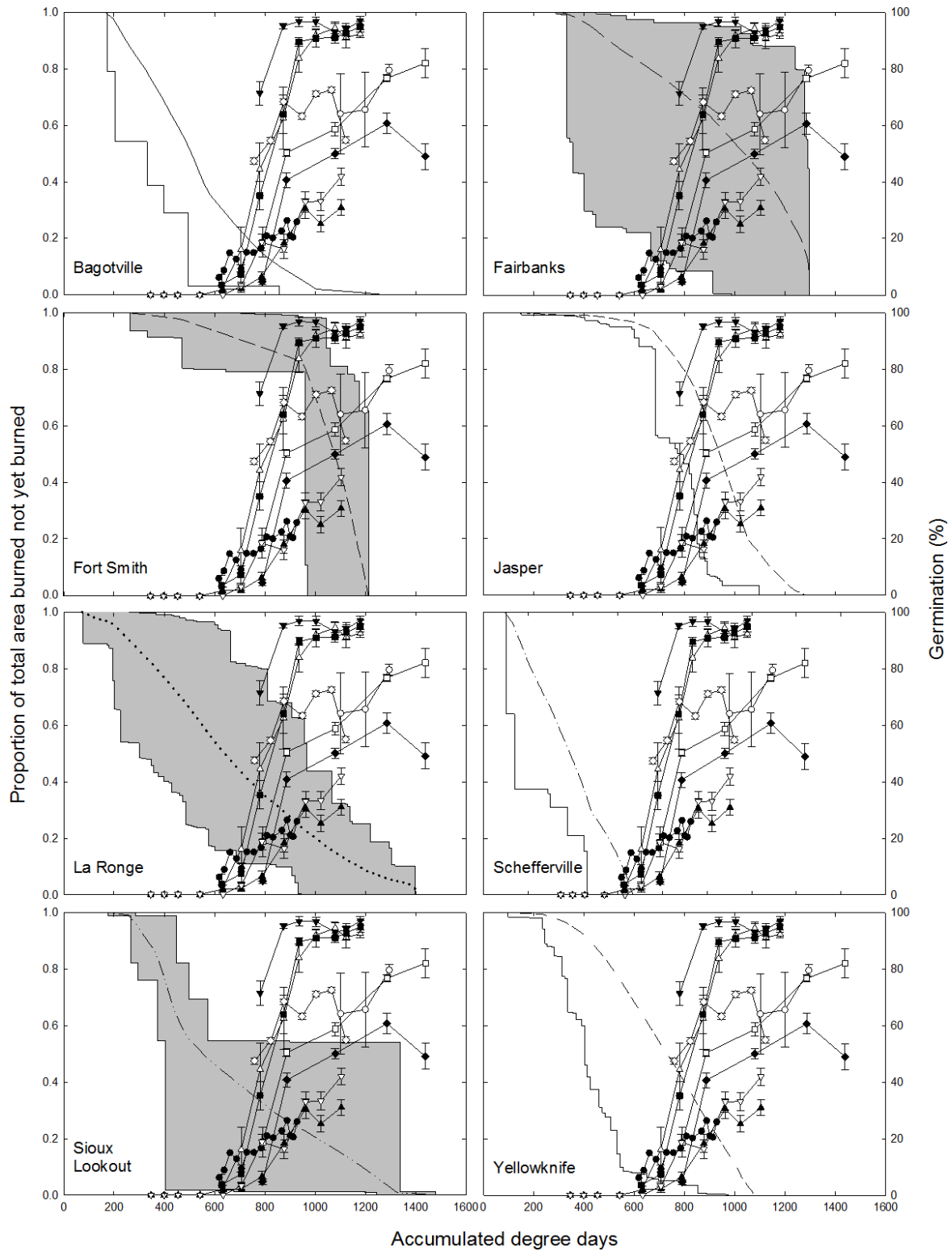


Figure I1: Timing of fire occurrence and seed development. For observation areas with fire end dates, grey areas define the space within which the actual distribution resides. The actual distributions are monotonically decreasing between the upper left and lower right corners of each area, and can be estimated by assuming the area burned by each fire occurs on the start date (left boundary), end date (right boundary), or by assuming steady state spread (center dashed lines) between start and end dates. For observation areas without fire end dates, distributions can be estimated assuming the area burned by each fire occurs on the start date (left-hand solid lines) or assuming steady state spread (right-hand lines) between start dates and estimated end dates (not shown; see methods). Error bars are standard error. ▲ Calgary, non-stratified (2010 data); ▽ Calgary, stratified (2010 data); ◆ Chalk River, non-stratified (Winston and Haddon, 1981); □ Chalk River, stratified (Winston and Haddon, 1981); ■ Fairbanks, non-stratified (Zasada, 1978); ▼ Fairbanks, stratified (Zasada, 1973); △ Fairbanks, stratified (Zasada, 1978); ○ Indian Head, stratified (Cram and Worden, 1957); ● Kananaskis Country (Crossley, 1953); ◇ Kananaskis Country, stratified (2006 data). Line styles for the distributions that were estimated using a steady state assumption correspond to those from Fig. 6.

Supplement J: Multiple regression analysis of time-integrated heat flux on cone surfaces as a function of cone heating time, cone height, and fire intensity.

Backwards stepwise multiple regression was used to relate time-integrated heat flux on cone surfaces (Fig. H1) to cone heating time, cone height, and fire intensity. The heating time for each cone was defined as the period for which total surface flux (sum of positive convective and radiative heat fluxes on the cone) was greater or equal to 1 kJ/m² and cone height was taken as 8.7 or 17.7 m (see methods).

In an attempt to identify relevant fire intensities (see discussion), three calculations were made for each cone: mean global intensity, flux-weighted global intensity, and mean local intensity. For mean and flux-weighted global intensities, global intensity I (kW/m) was first calculated for each time step i according to

$$I_i = \frac{\dot{Q}_i}{L} \quad (\text{J1})$$

where \dot{Q}_i is the total heat release rate (kW) and L is the fireline length in the y -direction (50 m).

Mean global fire intensity \bar{I} is then simply

$$\bar{I} = \frac{\sum_{i=1}^n I_i}{n} \quad (\text{J2})$$

where n is the number of time steps. Note that $i = 1$ corresponds to the time step where the total surface first flux exceeded 1 kJ/m² and n corresponds to the time step where the total surface flux

last fell below 1 kJ/m²; when this occurred more than once, i and n were based on the first and last instances, respectively. Flux-weighted global intensity was calculated as

$$I_w = \sum_{i=1}^n I_i \frac{q_i''}{q_1'' + q_2'' + \dots + q_n''} \quad (J3)$$

where q_i'' is the total surface flux (kJ/m²) at time step i . Thus, I_w is weighted in favor of those time steps for which total surface flux was greatest.

Mean local intensity was calculated using Eqns (J1) and (J2), except total heat release rate \dot{Q}_i was obtained for 12.5 x 12.5 x 40 m volumes around each cone array and the calculation considered only those time steps where \dot{Q}_i was greater than zero (12.5 m is a rough estimate of the average flame depth for the five crown fire simulations).

Statistical analyses were conducted using the statistical software R (R Development Core Team 2011). For flux-weighted global intensity, the variance of time-integrated surface flux was normalized using log₁₀-transformation. Multiple regression results are summarized in Table J1.

Table J1: Backwards Stepwise Multiple Regression Analysis of Time-Integrated Surface Flux as a Function of Cone Height, Heating Time, and Fire Intensity Calculated in Three Ways^a

Intensity calculation and variables	β	SE	<i>t</i>	<i>P</i>
Mean global intensity (model $F_{4,75} = 37.17, P < 0.001, R^2 = 0.65$)				
Heating time	18.480	4.543	4.07	<0.001
Height	-213.700	24.110	-8.87	<0.001
Intensity	0.051	0.019	2.64	<0.05
Heating time ²	-0.026	0.010	-2.63	<0.05
Flux-weighted global intensity (model $F_{5,74} = 31.25, P < 0.001, R^2 = 0.66$)				
Heating time	0.009	0.002	4.08	<0.001
Height	-0.063	0.010	-6.25	<0.001
Intensity	0.000	0.000	4.10	<0.001
Heating time ²	-0.000	0.000	-2.97	<0.01
Intensity ²	-0.000	0.000	-3.61	<0.001
Mean local intensity (model $F_{4,75} = 49.76, P < 0.001, R^2 = 0.71$)				
Heating time	3.124	1.191	2.62	<0.05
Height	-218.700	20.340	-10.75	<0.001
Intensity	2.029	0.396	5.12	<0.001
Intensity ²	-0.000	0.000	-4.26	<0.001

^aTable includes final models after removal of insignificant explanatory variables ($P \geq 0.05$).

Intercepts were significant for all models ($P < 0.0001$) and are not shown.

References

- Albini, F. A., and Baughman, R. G.: Estimating Windspeeds for Predicting Wildland Fire Behavior, USDA Forest Service Reserach Paper INT-221, 1979.
- Cram, W. H., and Worden, H. A.: Maturity of white spruce cones and seed, *Forest Science*, 3, 263-269, 1957.
- Crossley, D. I.: Seed maturity in white spruce, *Silviculture Research Notes No. 104*, Canada Department of Resources and Development, Forestry Branch, 1953.
- McGrattan, K., Hostikka, S., Floyd, J., Baum, H. R., Rehm, R. G., Mell, W. E., and McDermott, R.: *Fire Dynamics Simulator (Version 5) Technical Reference Guide Volume 1: Mathematical Model*, NIST Special Publications 1018-5, 2010.
- Winston, D. A., and Haddon, B. D.: Effects of early cone collection and artificial ripening on white spruce and red pine germination, *Canadian Journal of Forest Research*, 11, 817-826, 10.1139/x81-117, 1981.
- Zasada, J. C.: Effect of cone storage method and collection date on Alaskan white spruce (*Picea glauca*) seed quality, *Proceedings of the International Symposium on Seed Processing*, IUFRO, Bergen, Norway, 1973.
- Zasada, J. C.: Case history of an excellent white spruce cone and seed crop in interior Alaska: Cone and seed production, germination, and seedling survival, *US Forest Service General Technical Report PNW-65*, Portland, OR, 1978.